Materials Advances

ROYAL SOCIETY OF CHEMISTRY

PAPER

View Article Online
View Journal | View Issue

Cite this: *Mater. Adv.*, 2025, **6**, 7104

Thermal and rheological transitions of high performance semicrystalline polyaryletherketone (PAEK) polymers in material extrusion (MEX)

Melany McBean, *[a] Monis Luqman,[a] Nan Yi, *[a] Adam Chaplin[b] and Oana Ghita[a]

Mechanical properties in material extrusion (MEX) processes are influenced by the printing conditions and the cooling profile of extruded polymer. During cooling, the polymer transitions from a viscoelastic fluid to a "rubber" like state and ends as a glassy solid. The time taken to transition through each region is unique to individual polymers and it is linked to the melt rheology, thus indirectly affecting the layer to layer bond strength. By combining several thermal and thermomechanical methods, dynamic mechanical analysis (DMA), rotational rheometry (RR), differential scanning calorimetry (DSC) and infrared (IR) thermography, this paper defines the time a semicrystalline polymer takes to pass through each thermal transition region under a specific cooling regime. From the results, Victrex PAEK AM 200 spent 0.1 seconds in complete melt (terminal region), before beginning to solidify (rubbery region), taking a total of 0.95 seconds to reach complete solidification (glassy region). Defining these transition regions allows us to control the printing parameters for optimum interface bond strength, as the time spent in the terminal and rubbery regions governs interlayer diffusion. This is the first study to approach the combined melt rheology and solidification profile of a high-performance polymer in order to understand critical points within the printing process and identify ways of controlling them, providing quantitative values for the onset and endset of solidification of extruded polymer in MEX.

Received 9th July 2025,
Accepted 29th August 2025

DOI: 10.1039/d5ma00735f

rsc.li/materials-advances

1. Introduction

Material extrusion (MEX) is an additive manufacturing (AM) technique in which molten polymer is extruded through a nozzle and deposited onto a platform layer by layer in order to build a three-dimensional part. MEX is an attractive manufacturing method for the automotive, aerospace and biomedical industries due to its ability to build complex components with minimal lead time and the option of varied feedstock materials.[1] This enables the production of both prototypes and functional components with one manufacturing technique. Amongst the compatible feedstock materials are semicrystalline polymers. They exhibit excellent mechanical properties at high temperatures, as well as have good chemical and wear resistance.[2] Examples of these materials include Polyaryletherketones (PAEKs), which are a family of high temperature and performance polymers. Despite their improved properties and increased working temperature range, semi-crystalline polymers can be subject to shrinkage and warpage when compared to amorphous polymers.[3] These printing defects are generally caused by specific volume changes upon cooling, which are influenced by printing conditions.[3]

During MEX, the difference in temperature between the nozzle and chamber can generate rapid cooling profiles for the deposited polymer, generally in the span of seconds.[4] During this time, the polymer transitions from a molten viscoelastic fluid to a glassy solid, undergoing complete solidification.[5] In this study the terms solidification and cooling profile will be used to describe the physical and thermal changes occurring within the feedstock material from the moment of deposition. The cooling profile of a polymer is the change in temperature over time from the moment of deposition and is dependent on the set temperatures of the nozzle, chamber and platform in MEX. It has been obtained previously in the literature experimentally[6–8] and numerically[9–11] for various polymers. On the other hand, the solidification profile is based on the thermomechanical changes the polymer experiences upon cooling and is dependent on the molecular structure of the polymer.[12] It can be quantified by using the storage modulus (G'), which describes the elasticity of a polymer under dynamic stress. The changes in storage modulus of a polymer with temperature are inversely correlated with the free volume available and the chain mobility of the polymer's molecular

[a] *Faculty of Environment Science and Economy, University of Exeter, North Park Road, EX4 4QF, UK. E-mail: msm221@exeter.ac.uk, N.Yi@exeter.ac.uk*
[b] *Victrex Manufacturing Limited, Hillhouse International, Thornton Cleveleys, Lancashire FY5 4QD, UK*

structure.[13,14] A large number of papers[15–19] exist in the literature, in which the printing parameters and cooling conditions are related to the bond strength of printed parts. However, these conclusions are deduced relationships, lacking the understanding of the viscoelastic response to cooling of the polymers, and its impact on the bond formation between adjacent strands.[15–19] This paper proposes to provide these details and through this inform material and machine manufacturers on the design and set up of MEX processes.

Fig. 1 demonstrates the average changes in storage modulus and their corresponding regions of a viscoelastic polymer upon cooling.[12] During deposition the polymer is molten and deposited above its melting temperature (T_m) such that it can bond with the previously deposited layer.[20] Therefore, during deposition, the polymer is within the terminal region and acts as a viscoelastic fluid. Upon cooling, the polymer transitions into the rubbery region, becoming a ''rubber-like'' soft solid. The rubbery region is split into the rubbery plateau and transition region, behaving as a soft and stiff ''rubber-like'' material respectively. Upon further cooling, below the glass transition temperature (T_g), the polymer finally enters the glassy region and behaves like an elastic solid. Each transition from melt corresponds to an increase in storage modulus, which correlates to a decrease in free volume and chain mobility. Depending on its molecular structure, chain organisation and crystallite quantity, individual polymers will demonstrate unique thermal transitions.[12] Therefore, polymers subjected to the same cooling profile in MEX will not exhibit the same solidification profile.

The time spent in each thermal transition region is influenced by the cooling profile of the extruded polymer, which in turn is controlled by the selected printing parameters and the material's thermal properties. In two separate studies, T. Coogan, *et al.*[21] and Q. Sun, *et al.*[22] determined that by increasing the nozzle and chamber temperatures, the time taken to reach the glass transition temperature could be increased. This allowed for increased chain mobility and diffusion across the layer-to-layer interface, leading to increased bond strength.[21,22] From these studies, it can be concluded the time spent in each thermal transition region can be influenced by controlling the printing settings and thus the cooling profile. As each thermal transition region is related to changes in chain mobility and free volume, the time spent within the terminal and rubbery regions should be maximised for increased chain diffusion and therefore increased bond strength between adjacent layers.[20,23] However, in the terminal region, the viscosity is also at its lowest for the extruded polymer. C. Duty, *et al.*[5] determined that in order for a material to be printable, a stable geometry must be maintained upon deposition. Therefore, an extended time in the terminal region can cause excessive polymer flow, reducing dimensional fidelity. This demonstrates the need for a careful balance between the printing settings and the solidification profile of the polymer. In order to achieve this, the thermal transitions of the polymer in the MEX process need to be understood such that the time spent in the regions can be optimised.

The solidification profile of deposited polymers in MEX is not linear, rather it is dependent on its viscoelastic properties. Upon cooling, these thermal transitions govern the time adjacent strands are able to spend forming bonds. Therefore, understanding the time taken to reach each thermal transition from deposition is crucial to understanding the relationship between viscoelastic properties and filament bonding. In order to identify the thermal transition regions of cooling deposited filament, an experimental approach was taken. In this study, the thermal transition regions of a high temperature semi-crystalline polymer are quantitatively defined using dynamic mechanical analysis (DMA) and rotational rheometry (RR). The addition of the successive self-nucleation thermal data completes the solidification profile and adds significant insights into the rheological transitions taking place during cooling in MEX. This is the first study to experimentally determine the onset and endset of solidification, providing quantitative timings for the terminal, rubbery and glass transition regions of MEX extruded high-temperature semicrystalline polymer, forming the basis of a printing setting optimisation tool and informing the design and production of MEX tailored feedstock polymers.

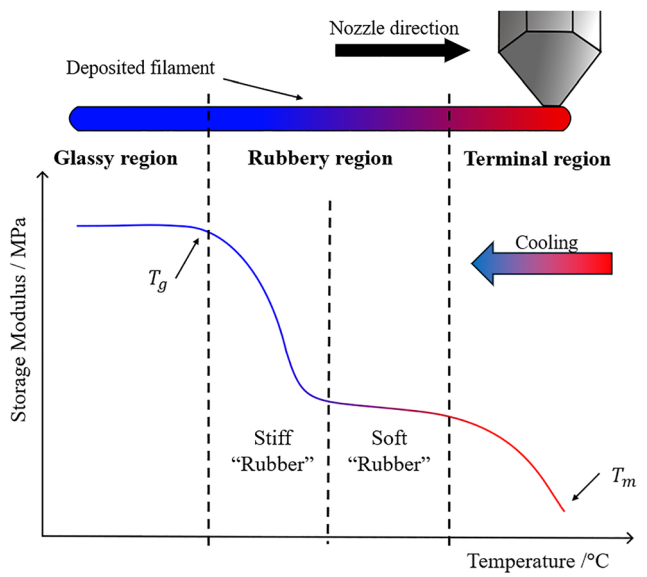

Fig. 1 Standard thermal transitions of polymers.

2. Materials

Victrex AM™ 200 was chosen for analysis in this study. It is a high performance, semi-crystalline PAEK co-polymer designed specifically for use in MEX printers. Table 1 outlines the

Table 1 Victrex PAEK AM 200 properties

Material	Manufacturer	Glass transition temperature [°C]	Melting temperature [°C]	Emissivity
PAEK	Victrex	150	303	0.63

Table 2 Printing settings used for Victrex PAEK AM 200 in a 3D Gence F340 MEX printer for infrared experiments

Settings	Values	Units
Nozzle temperature	400	°C
Print bed temperature	110	°C
Chamber temperature	35	°C
Print speed	25	mm s^{-1}
Layer height	0.3	mm
Layer time	15.8	s

properties of Victrex AM™ 200.[24] The emissivity for PAEK AM 200 listed in Table 1 was determined experimentally by Instrumentation Systems and Services (ISS).[25] Emissivity values are used to convert received energy values into temperature readings as IR cameras are not capable of directly reading temperature.[26]

3. Experimental methods

The thermal transition curve for polymers can be obtained over a range of temperatures using DMA and rheometry. However, due to the thermal hardware limitations, there is a gap in the test range between the two techniques. The Successive Self-nucleation and Annealing (SSA) protocol was used to provide data in this gap and therefore complete the full temperature region. Fig. 2 demonstrates the thermal transition captured by each method.

In order to determine the time spent in each thermal transition region, the cooling profile for PAEK AM 200 was obtained using an IR camera.

3.1. Dynamic mechanical analysis (DMA)

A Mettler Toledo DMA 1 was used to perform dynamic shear tests on crystalline PAEK AM 200 pellets. Dynamic shear tests were selected over alternative DMA test modes in order to have a direct comparison between rotational rheometry and DMA. Tests were conducted over a temperature range of 135–260 °C at a heating rate of 2 °C min^{-1}, a frequency of 1 Hz and an amplitude of 10 μm. Cylindrical pellet samples of AM200 with a diameter of 2 mm and a length of 3 mm were clamped using the shear titanium geometry. Tests were limited to 260 °C due to restrictions of the equipment.

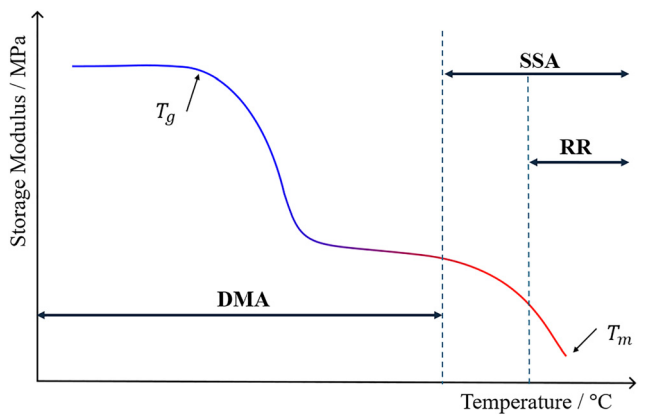

Fig. 2 Test ranges of dynamic mechanical analysis (DMA), rotational rheometry (RR) and successive self-nucleation and annealing (SSA) protocol.

3.2. Rotational rheometry (RR)

A TA Instruments DHR 1 rotational rheometer with 25 mm parallel plate geometry was used to conduct oscillatory temperature ramp tests on crystalline PAEK AM 200 chopped filaments over a temperature range of 310–330 °C at a heating rate of 2 °C min^{-1} and a frequency of 1 Hz. Tests on the rotational rheometer were limited to a start temperature of 310 °C due to a 50N axial force limit on the rheometer.

3.3. Successive self-nucleation and annealing protocol (SSA)

As the two methods, DMA and rheometry, cannot cover the entire temperature region and leave untested a temperature range gap between 260–310 °C a Successive Self-nucleation and Annealing (SSA) protocol was proposed with a Mettler Toledo DSC 1. This will allow the understanding of any crystal phase changes taking place close to the melt region. The Successive Self-nucleation and Annealing protocol (SSA) was created by A. J. Muller, *et al.* in 1997.[27] The technique consists of repetitive heating and cooling cycles within a DSC, designed to deconvolute melting endotherms into elementary components.[28] This process results in the definition of the self-nucleation domains (domains I–III) and a fractionated curve. Domain I (DI) occurs when the polymer is in complete melt and no crystals are present, (2) domain II (DII) where self-nucleation begins, and (3) domain III (DIII) where crystals are present in the melt. Prior to fractionating the curve, the first nucleation temperature ($T_{s,ideal}$) and the domain regions need to be identified. This is done by performing the self-nucleation protocol on the DSC, as outlined by B. Fillon, *et al.*[29] The self-nucleation protocol consists of conducting isothermal heating and cooling cycles on PAEK AM 200 at 10 °C min^{-1}, in order to capture the recrystallization curve shift in the cooling curve and the disappearance of the annealing peak in the melting curve. For PAEK AM 200, this range was 310–325 °C The $T_{s,ideal}$ was then used as the final isothermal temperature in the SSA protocol for AM 200, used to obtain a fractionated curve from 230–330 °C.

3.4. IR camera

An Optris Xi 400 IR camera was placed within the printing chamber of a 3D Gence F340 MEX printer in order to measure the deposition temperature and cooling curve of extruded PAEK AM 200 filaments. Table 2 outlines the printing setting used to print a double track "U" shaped part. Printing settings are standard for PAEK AM 200, apart from the chamber temperature which was reduced due to thermal restrictions of the IR camera.

Recordings of the printing process were taken on the Optris Xi 400 IR camera at a frequency of 40 Hz and a resolution of 382 × 288 and was analysed in the Optris PIX connect software. Temperatures were obtained by restricting the colour palette to display only the heat trail of the nozzle and extruded polymer.

4. Results and discussion

4.1. RR

Fig. 3 shows the storage modulus of PAEK AM 200 over a temperature range of 310–330 °C obtained using rotational rheometry (RR). Despite being above the melting temperature of AM 200, and well within the terminal region of the polymer, there is a change in storage modulus occurring between 314 °C and 319 °C. The storage modulus represents the elasticity of a polymer under dynamic stress and is inversely correlated with the free volume available and the chain mobility of the polymer's molecular structure.[13,14] Decreasing step changes (from lower to higher temperature) in the storage modulus are caused by relaxation transitions and phase transitions.[12] Thus, when considering higher to lower temperatures, step changes can be associated with chain stiffening, and chain mobility reductions. From higher temperatures, the increase in storage modulus seen in Fig. 3 between 319 and 314 °C, is the first instance of a step change occurring in storage modulus. This relates to an increase in energy storage and a reduction in chain mobility experienced by PAEK AM 200. As this is the first instance from higher temperatures, it can be considered as the onset of solidification of the polymer.

Factors such as the molecular weight and polymer architecture will impact the measured storage modulus. Materials with a higher molecular weight will demonstrate a higher storage modulus across all temperatures. On the other hand, materials with a higher degree of branching will impact chain mobility.

4.2 DMA

Fig. 4 and 5 show the storage modulus and phase angle of PAEK AM 200 over a temperature range of 135–260 °C. Phase angle or phase shift, is defined as the time lag between the applied stress and the corresponding strain and indicates whether a material behaves more like an elastic solid, or a viscous liquid. Phase angle varies between 0° to 90° where a value of 0° demonstrates that the material is ideally elastic, and a value of 90° demonstrates an ideally viscous fluid. Peaks in the phase angle represent structural changes occurring, such as the transition from solid to rubbery, and rubbery to viscous and correspond to steps in the storage modulus.

Due to noise present in the reading, the curve in Fig. 5 was smoothed using exponential smoothing, with a damping ratio of 0.9. From higher temperatures, in Fig. 4, the first increase in storage modulus occurs from 260 °C, which plateaus at approximately 230 °C. This is reflected as a phase angle peak in Fig. 5, with a maxima of 233 °C. The second change in storage modulus begins at 165 °C and plateaus at 150 °C, similarly, reflected as a peak in the phase angle curve, with a maxima of

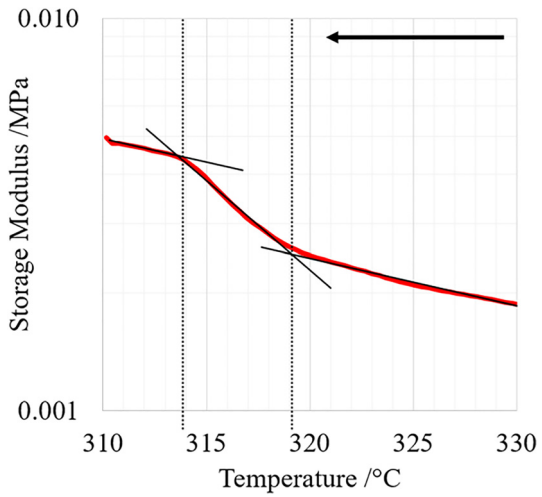

Fig. 3 RR Dynamic temperature ramp conducted on PAEK AM 200 from 310–330 °C.

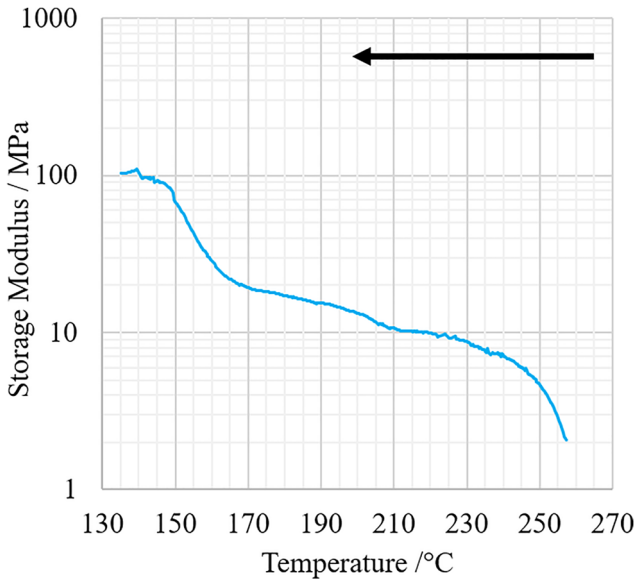

Fig. 4 DMA results for PAEK AM200 from 135–260 °C.

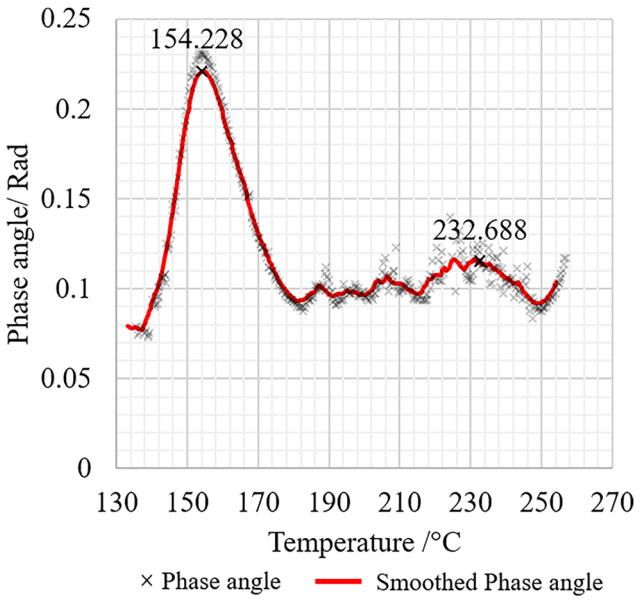

Fig. 5 Phase angle variance with temperature.

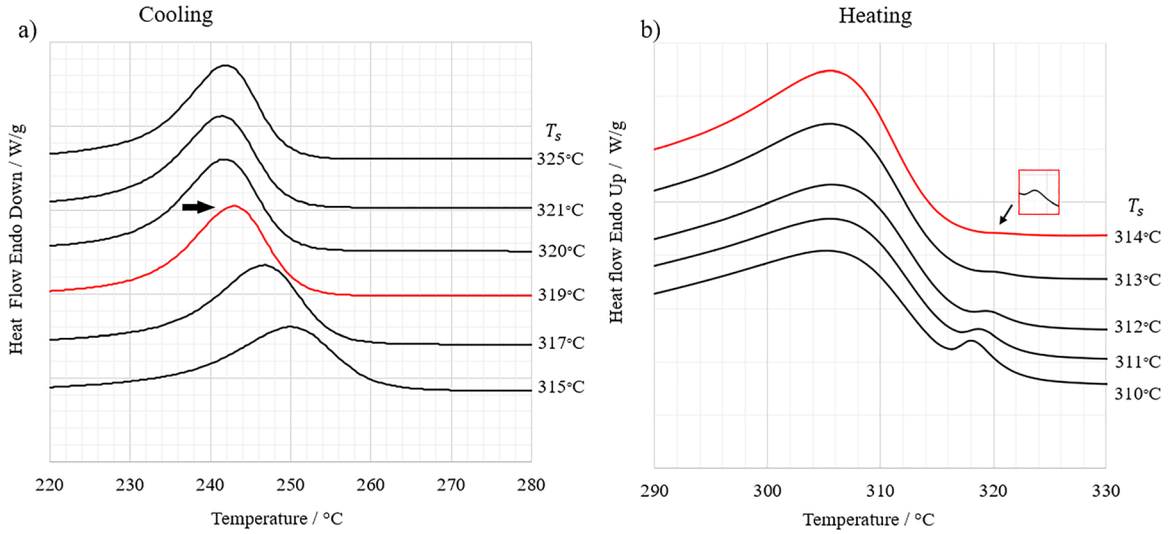

Fig. 6 (a) AM 200 cooling curves at 10 °C min^{-1} after 5 min at the indicated T_s. (b) AM 200 heating curves at 10 °C min^{-1} conducted after the cooling curves at 10 °C min^{-1}.

154 °C. The first increase in storage modulus can be attributed as the transition of the polymer from the terminal region to the rubbery plateau at 225 °C. The polymer then remains in the plateau until 165 °C at which point it enters the second transition region. The second increase in storage modulus therefore reflects the polymer transitioning from a "rubber" like polymer, to a glassy solid.

Factors such as the molecular weight and polymer architecture will impact the measured storage modulus in both RR and DMA techniques. Materials with a higher molecular weight will cause an increase in the length of the rubbery plateau towards higher temperatures,[12] whilst crosslinked materials, or materials with higher degree of branching will demonstrate a shallower rubbery transition curve. This is because branched chains act as cross links and impede the chains from moving, thus leading to a lower degree of relaxation in the chains.[30]

4.3. SSA

The SSA protocol was conducted on PAEK AM 200 in order to provide insight into the melt region and crystal melt temperatures. Fig. 6(a) shows the DSC cooling curves for AM 200 at 10 °C min^{-1} after being held at the T_s for 5 minutes, and Fig. 6(b) shows the subsequent heating curve of the sample at 10 °C min^{-1}. The ranges of the melt domains are obtained through qualitative analysis of the melting and cooling curves as outlined by B. Fillon, *et al.*[29] The upper range of DII is obtained by observing the first shift of the cooling curve towards higher temperatures, T_s = 319 °C for AM 200. The lower boundary of DII is obtained by observing the disappearance of the annealing peak in the melting curves. For AM 200, the peak was found to disappear after T_s = 314 °C, therefore, the lower bound of DII is 315 °C.

As per the SSA protocol by A. J Muller, *et al.*[28] the lower boundary of DII is the temperature at which crystals begin to form and is referred to as the $T_{s,ideal}$, which can be used as the first isothermal step in the protocol to obtain a fractionated crystal structure. Fig. 7 shows the SSA curve for AM 200 and lists the temperature ranges of the melt domains. The curve demonstrates a number of peaks, which represent crystal regions melting, with their size determining the proportion of crystals melting.[28] The largest portion of crystal melt occurs at 314 °C, just before the beginning of DII. As the polymer cools, it begins self-nucleating from 319 °C onwards. This can be taken as the onset of solidification, as chain mobility begins to reduce once crystals begin to form.

4.4. Complete solidification profile (T_g–T_m region)

Fig. 8 shows the combined SSA, DMA and RR dataset with the overlayed thermal transition regions. Within the terminal region of PAEK AM 200, there are the three melt domains, the ranges of which were obtained using the SSA protocol. From higher temperatures, DI ends at 319 °C (region 1), at which point self-nucleation begins (DII). From melt, the first crystal forms at 314 °C. This is matched by the rheometry dataset, which demonstrates an increase in storage modulus from 319–314 °C (region 2). This change can be attributed to the formation of the first crystal leading to a reduction in the chain mobility, and the free volume available. As this is the first significant increase in storage modulus experienced by the polymer from upon cooling, it can be considered as the onset of solidification for PAEK AM 200.

Upon further cooling (region 3), during DIII, there is a test gap between the DMA and RR testing ranges. However, the SSA results completes the range and shows the temperatures at which crystals begin to form. Each crystal formation can be associated with a further decrease in free volume, and thus chain mobility, leading to an increase in storage modulus per crystal formation. The terminal region of AM 200 ends at approximately 230 °C. This is supported by both the SSA

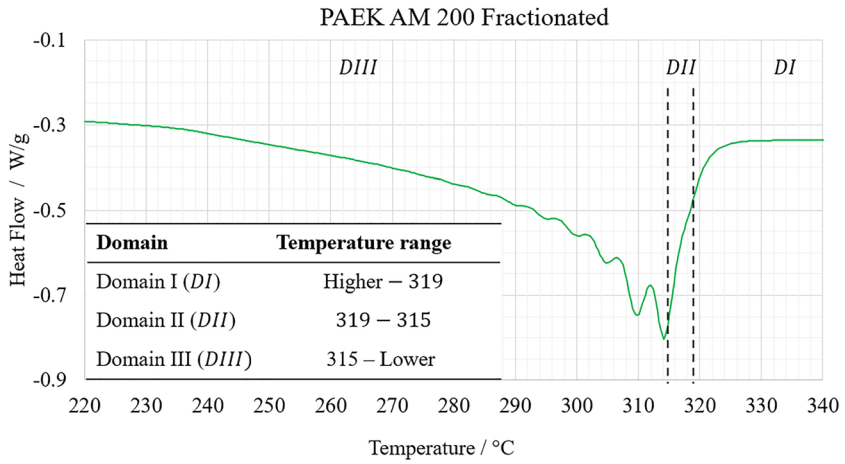

Fig. 7 AM 200 Fractionated DSC curve obtained using a $T_{s,ideal}$ of 315 °C.

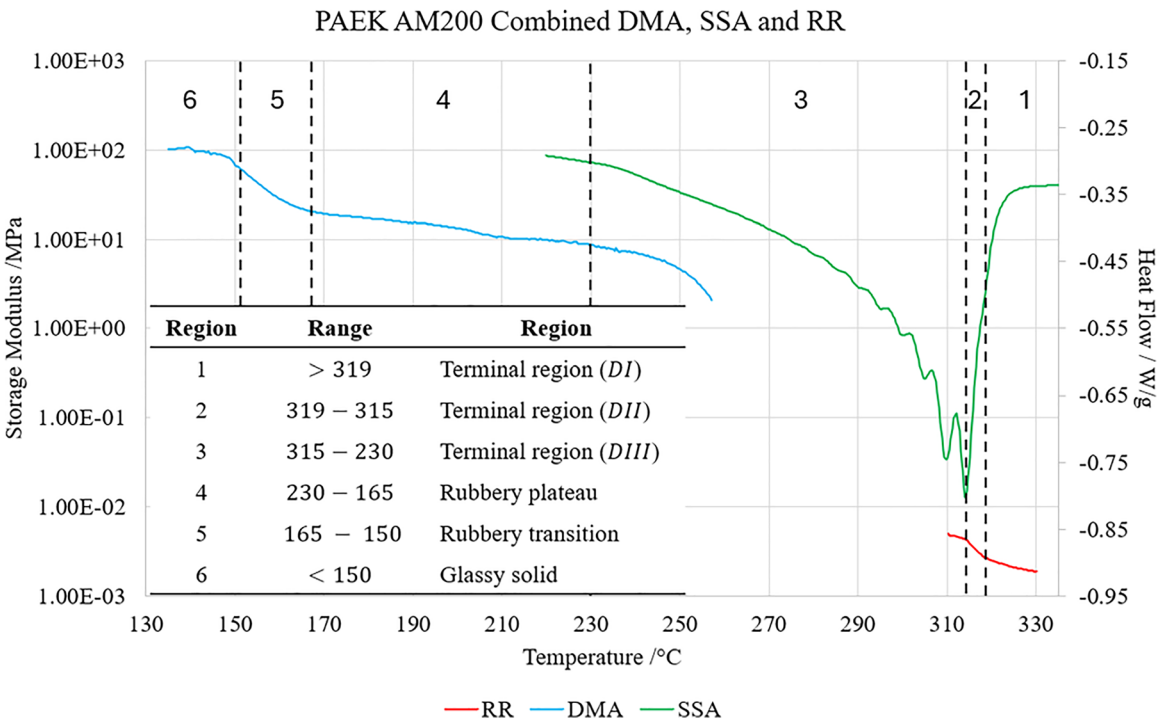

Fig. 8 Combined fractionated DSC curve with DMA and RR datasets.

protocol and DMA results, where a change in gradient is seen in both curves. The increase in storage modulus present in the DMA results, shows that the polymer melt is undergoing further hardening below the melt temperature and transitions from the terminal to the rubbery region, beginning to act as a soft "rubber-like" material.

Between the glass transition temperature (150 °C) and the onset of the terminal region (230 °C) (regions 4–5) the polymer is in the rubbery region. The behaviour of the polymer melt is further divided into soft and stiff "rubber-like" properties. Between 230–165 °C, the polymer is a soft "rubber", and experiences no significant changes in storage modulus, as it is within the rubbery plateau region. Once 165 °C is reached by the cooling melt, the polymer begins to enter its final increase in storage modulus before crossing the glass transition temperature and becoming a glassy solid (region 6). At this temperature, there is limited free volume available, with chain mobility at its minimum, and is therefore, the end of the solidification process.

4.5. Applicability of the viscoelastic curves in MEX

Fig. 9 presents the cooling profile of extruded PAEK AM 200 filament during the MEX process obtained *via* infrared thermography, as well as the deposition temperature and the time

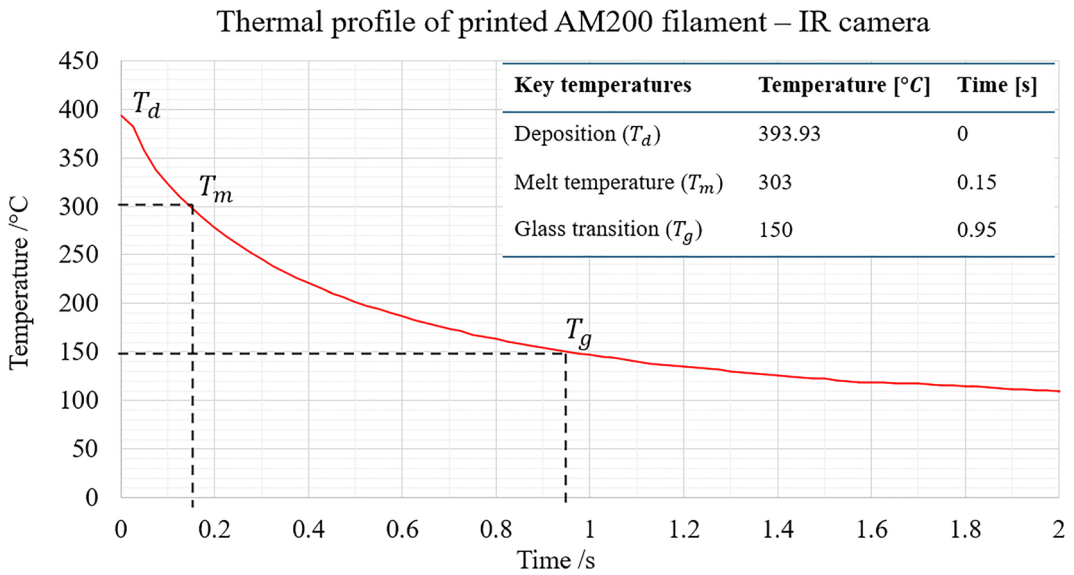

Fig. 9 Infrared cooling curve of MEX extruded PAEK AM 200 filament.

taken to reach the key temperatures listed in Table 1.[24] The temperatures were obtained by inputting an emissivity of 0.63, as shown in Table 1, to convert the IR recorded readings into true temperature values for PAEK AM 200. Materials with a higher emissivity will demonstrate lower overall temperatures, as the emissivity is tied to the amount of thermal energy a material reflects. The time axis has been adjusted such that the deposition begins at t = 0 s. At a nozzle temperature of 400 °C (Table 2), the deposition temperature at t = 0 s is 393.9 °C. The polymer then cools to the melt temperature within 0.15 seconds, after which the glass transition temperature is reached at 0.95 seconds. A further 1.5 seconds is taken to reach 100 °C.

The short cooling period experienced by PAEK AM 200 can be attributed to the low chamber temperature used in these experiments. A higher chamber temperature would lead to more gradual cooling, with more time taken to reach the melt and glass transition temperatures.[21,22] Each temperature boundary shown in Fig. 8 can be represented on the IR cooling curve as shown in Fig. 10. Table 3 summarizes the temperature ranges as well as the time spent in each thermal transition region. From the results, for the cooling profile generated by the printing settings, the time spent in complete melt is 0.1 seconds, at which point the polymer begins to solidify. The polymer remains in the melt region until 0.35 seconds. After this point the polymer enters the rubbery region for

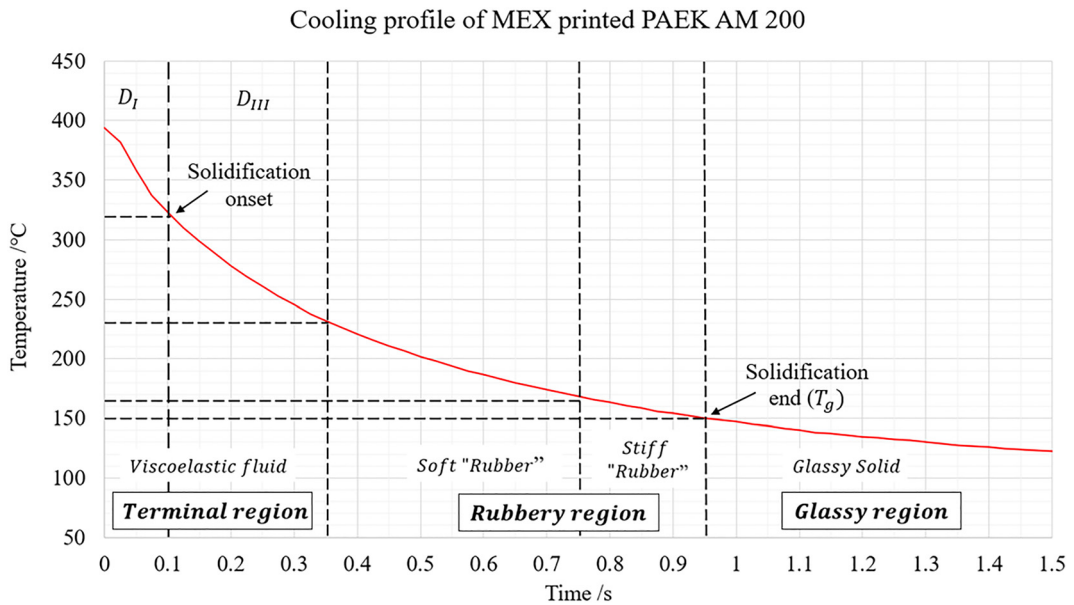

Fig. 10 Thermal transitions overlayed on MEX extruded PAEK AM 200 cooling curve.

Table 3 Thermal transition regions summary for PAEK AM 200 under specific cooling conditions

Key temperatures	Thermal transition region	Time range	Time spent
393.93–319	Terminal region – complete melt	0–0.1	0.1
319–230	Terminal region – solidification onset	0.1–0.35	0.25
230–165	Rubbery region – stable rubbery plateau	0.35–0.75	0.40
165–150	Rubbery region – rubbery transition to glassy state	0.75–0.95	0.2
>150	Glassy region	0.95+	—

0.40 seconds, before transitioning (0.80 s) to a glassy solid at 0.95 s.

During MEX, a polymer must be capable of holding its shape upon deposition[5,32] as well as form a bond with the previously deposited layer.[31,33] Therefore, in terms of thermal transitions during a print, the polymer should have a short complete melt region in order to avoid excessive flow and retain dimensional accuracy of the printed part, and the time spent in the terminal and rubbery regions should be maximised for increased diffusion across the layer. Having the thermal regions understood, the printing settings can be adjusted such that the time spent in each thermal transition region is optimized for bonding, stability and dimensional accuracy. By increasing printing settings such as the chamber temperature, the gradient of the cooling curve becomes more gradual, and therefore the polymer remains in the melt and rubbery plateau region for longer. From this, this study has the capacity to form the basis of a printing setting optimisation tool. Furthermore, as each polymer exhibits unique thermal transition regions, this methodology can also be used to form a criterion for designing polymers compatible with MEX printing. Therefore, by understanding the impact of the viscoelastic transitions of polymers in MEX, both commercial and academic users of MEX printers can benefit.

5. Conclusion

MEX extruded polymers begin to solidify in fractions of seconds. During solidification, a polymer undergoes various thermal transitions, during which the physical properties vary according to the viscous and elastic forces present at that temperature. The transitions can be split into three regions, the terminal, rubbery and glassy region. Each region corresponds to the polymer acting as a viscoelastic liquid, soft solid or elastic solid respectively. This study on additive manufacturing filament extrusion proposed a method in which the time spent in each thermal transition region was determined through a combination of thermal analysis, rheology and infrared thermography. This study quantified the time taken to reach the onset of solidification (0.1 s), and the time taken to reach complete solidification (0.95 s) for Victrex PAEK AM 200. By identifying the time taken to reach key transition temperatures this work has the potential to form the basis of a printing setting optimisation tool to improve part quality by informing users on target times spent in the terminal and rubbery regions, by way of controlling cooling profiles. Similarly, this study can inform MEX feedstock tailoring as each polymer demonstrates different transition region boundaries, with materials with a longer rubbery plateau and terminal transition allowing for more time for molecular diffusion and therefore interlayer bonding.

Author contributions

Melany McBean: writing – review & editing, writing – original draft, methodology, investigation, formal analysis, data curation, conceptualization, validation. Monis Luqman: data curation, formal analysis, methodology, validation. Nan Yi: supervision, writing – review & editing, investigation. Adam Chaplin: supervision, resources. Oana Ghita: writing – review & editing, validation, supervision, conceptualization.

Conflicts of interest

The authors declare that they have no known competing financial interests or personal relationships that could have appeared to influence the work reported in this paper.

Data availability

The data that support the findings of this study are openly available in Figshare at: **https://doi.org/10.6084/m9.figshare.29328434.v1**. This includes DMA, RR and SSA data, as well as Infrared cooling curves for Victrex PAEK AM™ 200.

Infrared cooling curves for Victrex PAEK AM™ 200 have also been included as supplementary information. See DOI: **https://doi.org/10.1039/d5ma00735f**.

Acknowledgements

This work was supported by Victrex Manufacturing Limited and the University of Exeter.

References

1 K. Sathish, S. S. Kumar, R. T. Magal, V. Selvaraj, V. Narasimharaj and R. Karthikeyan, *et al.*, A Comparative Study on Subtractive Manufacturing and Additive Manufacturing, *Adv. Mater. Sci. Eng.*, 2022, **2022**, 6892641, DOI: **10.1155/2022/6892641**.

2 C. Y. Li, The rise of semicrystalline polymers and why are they still interesting, *Polymer*, 2020, **211**, 123150. Available from: **https://www.sciencedirect.com/science/article/pii/S0032386120309757**.

3 D. Vaes and P. Van Puyvelde, Semi-crystalline feedstock for filament-based 3D printing of polymers, *Prog. Polym. Sci.*, 2021, **118**, 101411. Available from: **https://www.sciencedirect.com/science/article/pii/S0079670021000587**.

4 M. E. Mackay, The importance of rheological behavior in the additive manufacturing technique material extrusion, *J. Rheol.*, 2018, **62**(6), 1549–1561. Available from: https://pubs.aip.org/sor/jor/article/62/6/1549/1003019/The-importance-of-rheological-behavior-in-the.

5 C. Duty, C. Ajinjeru, V. Kishore, B. Compton, N. Hmeidat and X. Chen, *et al.*, What makes a material printable? A viscoelastic model for extrusion-based 3D printing of polymers, *J. Manuf. Process.*, 2018, **35**, 526–537. Available from: https://www.sciencedirect.com/science/article/pii/S1526612518311174.

6 R. B. Dinwiddie, V. Kunc, J. M. Lindal, B. Post, R. J. Smith and L. Love, *et al.*, Infrared imaging of the polymer 3D-printing process, *Thermosense: Thermal Infrared Applications XXXVI*, SPIE, Baltimore, 2014, p. 910502. Available from: https://www.spiedigitallibrary.org/conference-proceedings-of-spie/9105/910502/Infrared-imaging-of-the-polymer-3D-printing-process/10.1117/12.2053425.full?SSO=1.

7 E. Malekipour, S. Attoye and H. El-Mounayri, Investigation of Layer Based Thermal Behavior in Fused Deposition Modeling Process by Infrared Thermography, *Procedia Manuf.*, 2018, **1**, 1014–1022. Available from: https://www.sciencedirect.com/science/article/pii/S2351978918308096.

8 E. Ferraris, J. Zhang and B. Van Hooreweder, Thermography based in-process monitoring of Fused Filament Fabrication of polymeric parts, *CIRP Ann. Manuf. Technol.*, 2019, **68**(1), 213–216. Available from: https://www.sciencedirect.com/science/article/pii/S0007850619301556.

9 C. Basgul, F. M. Thieringer and S. M. Kurtz, Heat transfer-based non-isothermal healing model for the interfacial bonding strength of fused filament fabricated polyether-etherketone, *Addit. Manuf.*, 2021, **46**, 102097. Available from: https://www.sciencedirect.com/science/article/pii/S2214860421002621.

10 X. Zhou and S. J. Hsieh, Thermal analysis of fused deposition modeling process using infrared thermography imaging and finite element modeling, *Thermosense: Thermal Infrared Applications XXXIX*, SPIE, Anaheim, 2017, p. 1021409. Available from: https://www.spiedigitallibrary.org/conference-proceedings-of-spie/10214/1021409/Thermal-analysis-of-fused-deposition-modeling-process-using-infrared-thermography/10.1117/12.2262796.full.

11 J. Zhang, X. Z. Wang, W. W. Yu and Y. H. Deng, Numerical investigation of the influence of process conditions on the temperature variation in fused deposition modeling, *Mater. Des.*, 2017, **130**, 59–68. Available from: https://www.sciencedirect.com/science/article/pii/S026412751730521X.

12 K. P. Menard and N. R. Menard, Time and Temperature Scans Part I: Transitions in Polymers, *Dynamic Mechanical Analysis*, CRC Press, Boca Raton, 3rd edn, 2020, pp. 111–41. Available from: https://www.taylorfrancis.com/chapters/mono/10.1201/9780429190308-6/time-temperature-scans-part-transitions-polymers-kevin-menard-noah-menard.

13 H. Ramli, N. F. A. Zainal, M. Hess and C. H. Chan, Basic principle and good practices of rheology for polymers for teachers and beginners, *Chem. Teach. Int.*, 2022, **4**(4), 307–326. Available from: https://www.degruyter.com/document/doi/10.1515/cti-2022-0010/html?lang=en.

14 M. H. Cohen and G. S. Grest, Liquid-glass transition, a free-volume approach, *Phys. Rev. B*, 1979, **20**(3), 1077–1098, DOI: 10.1103/PhysRevB.20.1077.

15 D. Bhalodi, K. Zalavadiya and P. K. Gurrala, Influence of temperature on polymer parts manufactured by fused deposition modeling process, *J. Braz. Soc. Mech. Sci. Eng.*, 2019, **41**(113), 1–11, DOI: 10.1007/s40430-019-1616-z.

16 G. Dai, L. Zhan, C. Guan and M. Huang, The effect of cooling rate on crystallization behavior and tensile properties of CF/PEEK composites, *J. Polym. Eng.*, 2021, **41**(6), 423–430, DOI: 10.1515/polyeng-2020-0356/html.

17 H. R. Vanaei, M. Shirinbayan, S. F. Costa, F. M. Duarte, J. A. Covas and M. Deligant, *et al.*, Experimental study of PLA thermal behavior during fused filament fabrication, *J. Appl. Polym. Sci.*, 2021, **138**, e49747, DOI: 10.1002/app.49747.

18 C. Yang, X. Tian, D. Li, Y. Cao, F. Zhao and C. Shi, Influence of thermal processing conditions in 3D printing on the crystallinity and mechanical properties of PEEK material, *J. Mater. Process. Technol.*, 2017, **248**, 1–7. Available from: https://www.sciencedirect.com/science/article/pii/S0924013617301620.

19 R. Quelho de Macedo, R. T. L. Ferreira and K. Jayachandran, Determination of mechanical properties of FFF 3D printed material by assessing void volume fraction, cooling rate and residual thermal stresses, *Rapid Prototyp. J.*, 2019, **25**(10), 1661–1683. Available from: https://www.emerald.com/rpj/article-abstract/25/10/1661/369464/Determination-of-mechanical-properties-of-FFF-3D?redirectedFrom=fulltext.

20 C. Bellehumeur, L. Li, Q. Sun and P. Gu, Modeling of Bond Formation Between Polymer Filaments in the Fused Deposition Modeling Process, *J. Manuf. Process.*, 2004, **6**(2), 170–178. Available from: https://www.sciencedirect.com/science/article/pii/S1526612504700717.

21 T. F. Coogan and D. O. Kazmer, Healing simulation for bond strength prediction of FDM, *Rapid Prototyp. J.*, 2017, **23**(3), 551–561. Available from: https://www.emeraldinsight.com/1355-2546.htm.

22 Q. Sun, G. M. Rizvi, C. T. Bellehumeur and P. Gu, Effect of processing conditions on the bonding quality of FDM polymer filaments, *Rapid Prototyp. J.*, 2007, **14**(2), 72–80. Available from: https://www.emerald.com/rpj/article-abstract/14/2/72/365935/Effect-of-processing-conditions-on-the-bonding?redirectedFrom=fulltext.

23 Y. S. Ko, D. Herrmann, O. Tolar, W. J. Elspass and C. Brändli, Improving the filament weld-strength of fused filament fabrication products through improved interdiffusion, *Addit. Manuf.*, 2019, **29**(100815), 1–8. Available from: https://www.sciencedirect.com/science/article/pii/S2214860419303203?via%3Dihub.

24 Victrex. Victrex Technical Datasheets. 2024 [cited 2024 May 13]. VICTREX AMTM 200 FIL. Available from: https://www.victrex.com/en/downloads/datasheets/victrex-am-200-fil.

25 Instrumentation Systems and Services Ltd. [cited 2024 Nov 22]. Available from: **https://www.issltd.co.uk/**.

26 R. P. Madding, Emissivity measurement and temperature correction accuracy considerations, *Proc. SPIE*, 1999, **3700**, 393–401, DOI: **101117/12342307**, **https://www.spiedigitallibrary.org/conference-proceedings-of-spie/3700/0000/Emissivity-measurement-and-temperature-correction-accuracy-considerations/10.1117/12.342307.full**.

27 A. J. Müller, Z. H. Hernández, M. L. Arnal and J. J. Sánchez, Successive self-nucleation/annealing (SSA): A novel technique to study molecular segregation during crystallization, *Polym. Bull.*, 1997, **39**(4), 465–472, DOI: **10.1007/s002890050174**.

28 A. J. Müller, R. M. Michell, R. A. Pérez and A. T. Lorenzo, Successive Self-nucleation and Annealing (SSA): Correct design of thermal protocol and applications, *Eur. Polym. J.*, 2015, **65**, 132–154. Available from: **https://www.sciencedirect.com/science/article/pii/S0014305715000270**.

29 B. Fillon, J. C. Wittmann, B. Lotz and A. Thierry, Self-nucleation and recrystallization of isotactic polypropylene (α phase) investigated by differential scanning calorimetry, *J. Polym. Sci., Part B: Polym. Phys.*, 1993, **31**(10), 1383–1393, DOI: **10.1002/polb.1993.090311013**.

30 C. W. Macosko, Rheology of Polymeric Liquids, *Rheology – Principles, Measurements and Applications*, Wiley-VCH, New York, 1994, pp. 475–514.

31 L. Li, Q. Sun, C. Bellehumeur and P. Gu, Investigation of Bond Formation in FDM Process. In: 2002 International Solid Freeform Fabrication Symposium. Austin; 2002 [cited 2025 Aug 18]. p. 400–7. , DOI: **10.26153/tsw/4500**.

32 J. Vlachopoulos and D. Strutt, The Role of Rheology in Polymer Extrusion. In: New Technology for Extrusion Conference. Milan; 2003 [cited 2024 Apr 29]. p. 1–25. Available from: **https://www.researchgate.net/profile/John-Vlachopoulos/publication/266472193_The_Role_of_Rheology_in_Polymer_Extrusion/links/54c30c910cf256ed5a904ada/The-Role-of-Rheology-in-Polymer-Extrusion.pdf**.

33 C. T. Bellehumeur, M. Kontopoulou and J. Vlachopoulos, The role of viscoelasticity in polymer sintering, *Rheol. Acta*, 1998, **37**(3), 270–278, DOI: **10.1007/s003970050114**.